Nonlinear FDTD Simulation of Optical Thin Films with Intensity-Dependent Drude-Lorentz Parameters

João G. Nizer Rahmeier, Tom. J. Smy and Shulabh Gupta
Department of Electronics, Carleton University, Ottawa, Ontario, Canada.
Email: joaonizer@cmail.carleton.ca.

***Abstract*— Nonlinear optical materials, such as transparent conductive oxides, have recently drawn a lot of attention when being integrated into metasurfaces and allowing full-optical control of the surface response. Although several methods for modeling the nonlinear materials have been proposed in the literature, most of them have the limitations on being non-dispersive and of instantaneous response. In this paper, we present a straightforward integration of an extended Drude-Lorentz model that captures the local intensity response of nonlinear materials while being dispersive and allowing for inertial response via a low-pass filtering process. This method is integrated into standard finite-differences time-domain (FDTD) implementation of Maxwell's equations and the auxiliary differential equations approach of the Drude-Lorentz model is extended via local intensity-dependent parameters. A numerical demonstration shows the response for a thin film of nonlinear material, where the parameters across the sample are time-varying with respect to the local intensity of the fields. Therefore, showing a direct feedback of the field profile to the nonlinear response of the material, which is critical when incorporating such films in resonating meta-atoms.**

I. Introduction

Metasurfaces are defined, in general, as a 2D arrangement of 3D sub-wavelength scatterers. Their sub-wavelength features are engineered so that when interacting with an incident wave, they allow phase, amplitude and polarization changes while operating in a reflection or transmission regime [1]. Nonlinear optical metasurfaces have drawn a lot of attention in recent years due to their capability to allow full-optical dynamic control of the response of the metasurface unit cell exploiting nonlinear responses of novel optical materials [2]–[5].

In terms of nonlinear materials, transparent conductive oxides (TCOs), such as indium tin oxide (ITO) and aluminum-doped zinc oxide (AZO), are of particular interest in recent applications due to their low absorption of electromagnetic waves within the visible region [6], large changes in their permittivity when excited close to their epsilon-near-zero (ENZ) frequency [7], fast response in the order of hundreds of femtoseconds [8] and broadband frequency translation through time refraction [9]. In the case of ITO, for example, its nonlinear response is usually characterized using a pump-probe experiment, where the permittivity is observed to change as a function of the pump intensity in free-space [10]. Its permittivity response can then be further represented in a non-dispersive susceptibility (χ)-model, where the polarization response at a particular frequency is expanded as a power series in terms of the electric field. Moreover, this type of model has shown that nonlinear susceptibility terms up to the seventh order can be required for an appropriate representation of the nonlinear phenomena at high pump intensities [11]. While insightful, this approach is not particularly interesting for a time-domain full-wave electromagnetic simulation of the nonlinear material because it is a non-dispersive model and its dispersive counterpart would require complex convolution evaluations, increasing the computational memory requirements. This in turn, is a limiting factor for simulations of optical nonlinear metasurface structures that by default require finer meshes to resolve sub-wavelength features and smaller step-sizes to resolve higher-order harmonics of the fields.

Current limitations in nonlinear material models are related to simple non-dispersive cases [12], [13], instantaneous response where the modulation signal is independent of local field enhancement effects [14], limitations to third-order susceptibility only [15], [16] and the low perturbation expansion of the anharmonic Lorentz resonator that is reported to be unstable at particular nonlinear conditions [17]. An insightful model, based on experimental results, is proposed in [10] for an ITO slab, where the nonlinear response of the material with respect to the pump intensity is characterized in terms of a change in the effective mass and mobility of the electrons. Assuming that the electron density is conserved under intraband transitions, these parameters are then responsible for determining the plasma frequency and the dumping frequency in the Drude-Lorentz model. Therefore, plasma frequency and dumping frequency can be seen as time-dependent variables whose time dependence comes from the varying field intensity of the pump signal. Still, this correspondence is limited by the fact that local field enhancements on resonating structures would not affect the parameters of the extended model since it is currently defined in terms of the pump intensity in free space. We attempted implementing an intensity-dependent material plugin in the Flexible Material Plugin Framework of Ansys/Lumerical [18], however, direct access to E and H fields at a particular Yee cell was not available, limiting the implementation to something that was close to the implementation in [8] for a time-varying permittivity, without direct feedback from local electromagnetic field interactions.

Hence, there is a clear need to develop an intensity-dependent dispersive model of nonlinear materials which takes into account the local field enhancement effects and

thus the local response of the material. Therefore, in this work, we have incorporated time-dependent parameters in the Drude-Lorentz model to characterize the intensity-dependent local response of nonlinear materials. These parameters are defined as a polynomial expansion in terms of the magnitude of the Poynting vector at the Yee cell level. This thus enables the integration of a dispersive, non-instantaneous intensity-dependent time-varying local response of nonlinear materials in an FDTD electromagnetic solver.

II. Dispersive Nonlinear Model

A. Intensity-Dependent Drude-Lorentz Model

A flexible form to represent the permittivity of a dispersive material is to use the Lorentz oscillator model [19], that in the time domain corresponds to the following second-order differential equation:

$$\frac{\partial^2 \mathbf{P}}{\partial t^2} + \gamma \frac{\partial \mathbf{P}}{\partial t} + \omega_0^2 \mathbf{P} = \epsilon_0 \omega_p^2 \mathbf{E}. \tag{1}$$

where ω_p is the plasma frequency, γ is the damping frequency, and ω_0 is the resonance frequency. For a linear system, these parameters are constants that characterize a resonant response, and in a more specific case, where no resonance is present within the frequency of interest ($\omega_0 = 0$), this model corresponds to a Drude response. Hence, we refer to this model as a Drude-Lorentz model.

Assuming a low-density approximation of the carriers, where the dynamic of one electron is independent of other electrons even in the presence of a modulating signal, we can then write the Drude-Lorentz model in (1) with time-dependent parameters

$$\frac{\partial^2 \mathbf{P}}{\partial t^2} + \gamma(t) \frac{\partial \mathbf{P}}{\partial t} + \omega_0(t)^2 \mathbf{P} = \epsilon_0 \omega_p(t)^2 \mathbf{E} \tag{2}$$

where

$$\begin{aligned} \omega_p(t) &= f_{\omega_p}(I) \\ \gamma(t) &= f_{\gamma}(I) \\ \omega_0(t) &= f_{\omega_0}(I) \end{aligned} \tag{3}$$

are now functions of the local intensity

$$I(x, y, z, t) = \frac{1}{2} |\mathrm{Re}\{\mathbf{S}(x, y, z, t)\}|^2 \tag{4}$$

where $\mathbf{S} = \mathbf{E} \times \mathbf{H}^*$ is the Poynting vector.

The forms of $f(I)$ in (3) are arbitrary in general, and in this paper, we chose it to be of a polynomial form,

$$f(x) = a_n x^n + \ldots + a_1 x + a_0, \tag{5}$$

due to the characteristics of the experimental data used later on during the numerical demonstration in Sec. III. Together, (2), (3) and (4) allows us to describe an intensity-dependent dispersive material response due to a local change in the intensity. While a time-varying intensity dependence is chosen here to illustrate the method, the upcoming FDTD simulation framework is capable of user-defined time-dependence of the Lorentz-Drude parameters.

B. Dynamic Response of the Material

Experimental data for ITO, for example, shows that the change in the material properties with respect to intensity is not instantaneous. It actually follows an exponential decay after the high-intensity pump signal ceases to interact with the nonlinear material [10], corresponding to a delayed response. The instantaneous intensity in (4) has an angular frequency that is twice that of the interacting fields. Hence, the local intensity used to determine the parameters in (3) has to go over a low-pass filtering process that will capture this inertia (or "memory") of the material while responding to an instantaneous change in the local intensity.

The low-pass filtering step can be represented using a filter that is suitable for the physical process controlling the dynamic response. In this work, for simplicity and motivated by the simple form of the decay, we are going to consider a first-order low pass filter, i.e., a single-stage RC filter of the form,

$$\tau \frac{\partial I_{\mathrm{lc}}(x, y, z, t)}{\partial t} + I_{\mathrm{lc}}(x, y, z, t) = I \tag{6}$$

where τ is the time constant of the filter and I_{lc} is the local slowly varying intensity perceived by the material at a given time instant. A discretized version of this system can be written as

$$I_{\mathrm{lc}}^n = \alpha I^n + (1 - \alpha) I_{\mathrm{lc}}^{n-1} \tag{7}$$

where n is the time index and α is the inertial factor directly related to the time-step, Δ_t and the time constant, τ via $\alpha = \Delta_t / (\tau + \Delta_t)$.

In general, this filtering step can be extended to higher-order filters at the expense of computational resources. Moreover, different parameters in (3) can possess different time responses for each of the three Lorentz-Drude Parameters [10]. Therefore, separate filtering processes with different time constants can easily be incorporated into the proposed numerical framework.

C. FDTD Implementation

A 3D finite-differences time-domain (FDTD) solver of Maxwell's equations was implemented in Matlab using standard FDTD techniques, and the Drude-Lorentz model in (1) was implemented using auxiliary-differential equations (ADE), both using standard techniques available in [20] and [21].

Extension of (1) to (2) via (3) requires the Poynting vector calculation at the center of each Yee cell that constructs the nonlinear material. It happens at each integer time-step, right-before updating the polarization term with the current values of the E-field. However, as depicted in Fig. 1, E-field nodes in the Yee cell must be centered at the (i, j, k) position by taking the average of the four field components at the edges of the Yee cell. Thus, constructing the electric field vector,

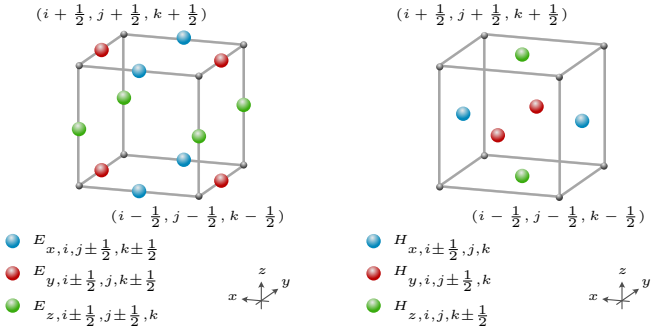

Fig. 1. Black spheres at half space-steps represent the nodes forming a particular Yee cell at position (i, j, k). E-field nodes are located at the center of each edge, and H-field nodes are placed at the center of each face. E and H fields are half a time-step apart from each other.

$\mathbf{E}^n_{i,j,k}$. For example, E_x is

$$E^n_{x,i,j,k} = \frac{E^n_{x,i,j-\frac{1}{2},k-\frac{1}{2}} + E^n_{x,i,j-\frac{1}{2},k+\frac{1}{2}}}{4} + \frac{E^n_{x,i,j+\frac{1}{2},k-\frac{1}{2}} + E^n_{x,i,j+\frac{1}{2},k+\frac{1}{2}}}{4} \tag{8}$$

Similarly, the H-field nodes are located at the center of the faces of the cell and are half a time-step apart from the E-field. Thus, in total, we require the averaging of another four field components at two spatial positions (i.e., $i+\frac{1}{2}$ and $i+\frac{3}{2}$ for H_x) and two time-instants $(n-\frac{1}{2}, n+\frac{1}{2})$. Hence, constructing the magnetic field vector, $\mathbf{H}^n_{i,j,k}$. For example, $H^n_{y,i,j,k}$ is

$$H^n_{y,i,j,k} = \frac{H^{n-\frac{1}{2}}_{y,i,j-\frac{1}{2},k} + H^{n-\frac{1}{2}}_{y,i,j+\frac{1}{2},k}}{4} + \frac{H^{n+\frac{1}{2}}_{y,i,j-\frac{1}{2},k} + H^{n+\frac{1}{2}}_{y,i,j+\frac{1}{2},k}}{4} \tag{9}$$

After that, the Poynting vector and the local intensity in (4) can be calculated and determined at the center of all nonlinear material cells using co-located $\mathbf{E}$ and $\mathbf{H}$ field vectors. Subsequently, this local intensity is fed through the low-pass filter, i.e. (7) and its filtered output, I_{lc} is further used in the polynomial expansions, $f(I_{\text{lc}})$ in (3) for appropriate Drude-Lorentz intensity-dependent parameter calculation.

Since the electric polarization terms are co-located with the E-field nodes in the Yee cell, we need to perform a final averaging over ω_p, γ and ω_0 in order to convert them back to the E-field node positions at the edges of the Yee cell. For simplicity, nodes at the edge of the material boundaries are kept equal to the values at the center of the Yee cell they belong, and nodes in between Yee cells are computed as the average of the values of the four surrounding cells. Finally, we proceed by updating the electric polarization terms and calculating the future values of the E-field, following the standard marching loop of the FDTD Yee-cell solver.

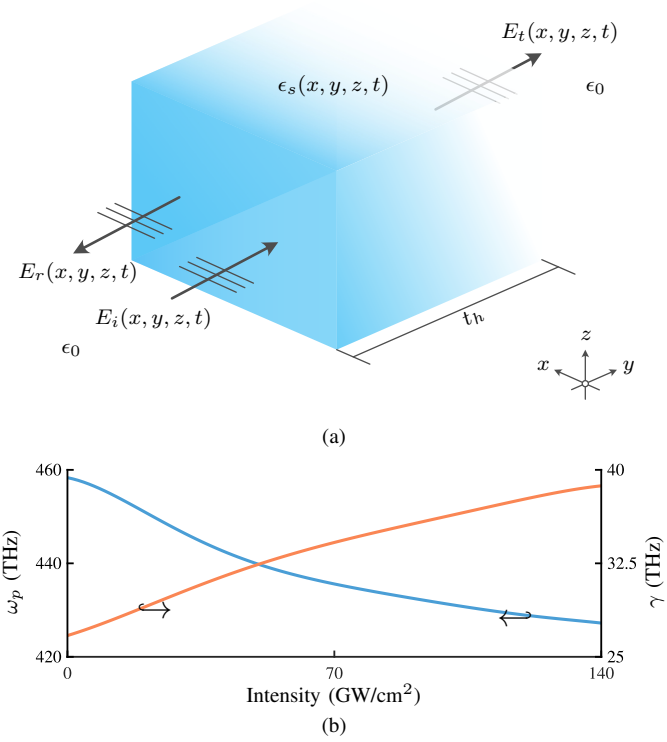

Fig. 2. Simulation setup. (a) Material slab with intensity-dependent permittivity,ϵ_s and two semi-infinite free space mediums, ϵ_0. (b) Intensity-dependent profile of plasma frequency, ω_p (left) and damping frequency, γ (right). The profile is represented using a polynomial expansion of the seventh order.

III. Numerical Demonstration

Consider the semi-infinite ENZ slab presented in Fig. 2(a). The slab is 220 nm thick along the z-direction, and its permittivity is defined by a Drude response ($\omega_0 = 0$) whose ω_p and γ are both functions of intensity, and their profile is represented in Fig. 2(b). The intensity-dependent parameters are represented using a polynomial expansion of $f()$ in (3) with order 7 for both ω_p and γ. These values are obtained from [10] for a 220 nm thin film of ITO, and the intensity, in that case, is the pump free-space intensity, whereas here, due to the modeling we are developing, it is considered to be the local intensity at the center of each Yee cell. It is our understanding that this equivalence between free space pump intensity and local intensity is not true in general, but overall it serves the purpose of a numerical demonstration. Also, the memory of the material response with respect to intensity is modeled using a first-order system with a damping factor $\alpha = 0.995$. The time-domain representation of the incident field is shown in Fig. 3(a) along with its spectrum. It is a Gaussian pulsed plane-wave centered at 246 THz, with a pulse length of 75 ps, a standard deviation of 63.7 ps, and the amplitude for the high-intensity response is 8.97 MV/cm which would correspond to a maximum intensity of 140 GW/cm^2 inside the material if all power would get

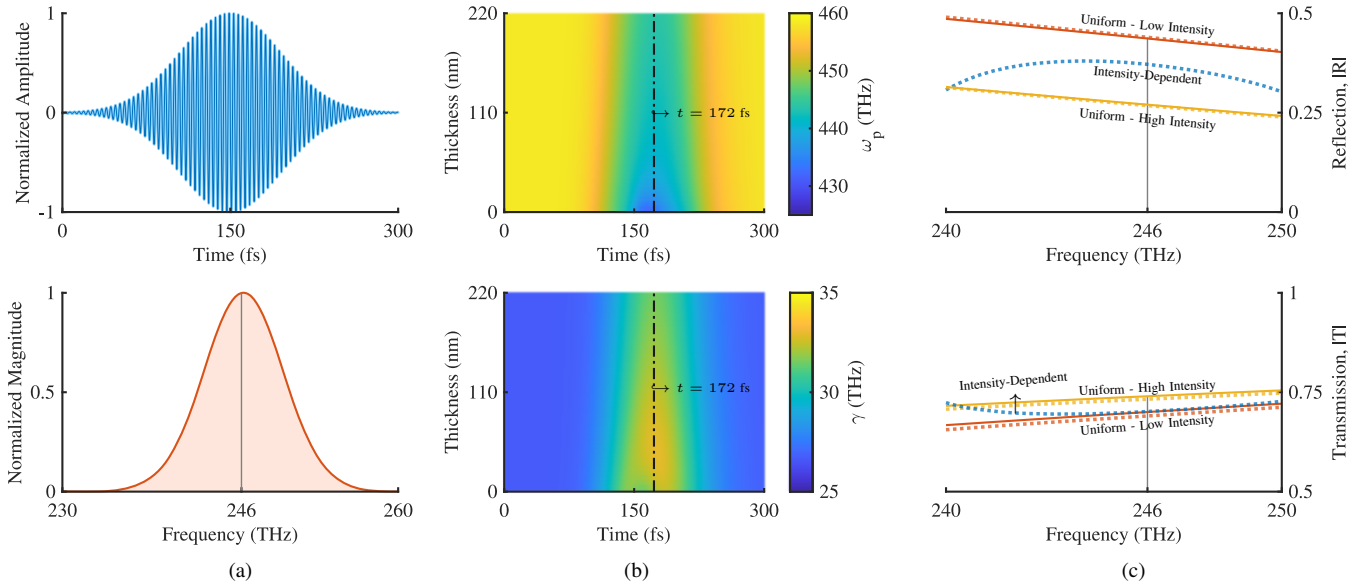

(a) (b) (c)

Fig. 3. Simulation setup and numerical results. (a) Incidence field in the time and frequency domain, centered at 150 fs and 246 THz, respectively. (b) The evolution of the Drude parameters across the thickness of the nonlinear slab as a function of time. (c) The magnitude of the reflection and transmission coefficients. Fresnel coefficients (solid lines) are calculated using an isotropic uniform Drude media with fixed parameters at a low or high intensity. FDTD results (dashed lines) are shown for comparison. The blue curve corresponds to the intensity-dependent simulation, while red and yellow represent the isotropic uniform Drude response at low and high intensity, respectively.

transmitted through the slab.

Figure 3(b) shows the change in ω_p and γ across the thickness of the slab with respect to time. Initially, the intensity is low all over the sample, and the parameters stay at their low-intensity values. As the plane-wave increases in amplitude, its interaction with the sample causes the parameters to change, ω_p decreases and γ increases as defined by the profile in Fig. 2(b). Once the signal's amplitude gets reduced, the sample return to its low-intensity state. It is worth noticing that the first-order low pass filtering in the intensity calculation allows for the representation of the memory mechanism in the material response, which can be seen in Fig. 2(b) as the peak material response at 172 fs does not coincide with the peak incident field intensity at 150 fs.

Figure 2(c), shows the magnitude of the reflection and transmission coefficients for the intensity-dependent response (dashed-blue) in comparison with those of a uniform media at low-intensity ($\omega_p = 458.3$ THz and $\gamma = 26.7$ THz) high intensity ($\omega_p = 427.3$ THz and $\gamma = 38.7$ THz) calculated using Fresnel equations (solid-red and yellow) and regular FDTD-ADE (dashed-red and yellow). The dynamic response shows a reflection magnitude within the low-high intensity limits. However, transmission is roughly the same as that of a uniform low-intensity slab around the center frequency, resulting in an increased absorption during the dynamic change of the permittivity profile across the sample. Moreover, the result shows the dispersive characteristics of the material. Therefore, highlighting the importance of a non-instantaneous dispersive intensity-dependent model for nonlinear thin films.

IV. Conclusion

In this paper, we presented the initial steps for modeling the dynamic response of general nonlinear materials, such as ENZ materials, via a local intensity-dependent Drude-Lorentz model. A numerical demonstration shows the material properties changing across a thin film of nonlinear material as a normal incident pulsed plane-wave propagates through it. Due to the memory mechanism implemented via a first-order low pass filter, the response is delayed, which reflects realistic effects observed in experiments. Moreover, due to the relatively short length of the incident pulse, we ended up characterizing the transmission and reflection of a transient response, where neither reflection nor transmission directly corresponds with those of a static low/high intensity response obtained via Fresnel equations corresponding to a linear system, as expected. Reflection magnitude was in-between the two limits, however, the transmission was somewhat smaller around the center frequency due to absorption caused by the time-changing permittivity profile across the sample. A natural extension of this work is to establish a relationship between the free-space intensity and the local intensity calculated inside the materials using the Poynting vector and general field components. Furthermore, the model can be validated for other nonlinear effects such as self-focusing, frequency generation and time-refraction.

References

[1] V.-C. Su, C. H. Chu, G. Sun, and D. P. Tsai, "Advances in optical metasurfaces: fabrication and applications," *Opt. Express*, vol. 26, no. 10, pp. 13 148–13 182, May 2018.

[2] A. Krasnok, M. Tymchenko, and A. Alù, "Nonlinear metasurfaces: a paradigm shift in nonlinear optics," *Materials Today*, vol. 21, pp. 8–21, 2018.

[3] J. G. N. Rahmeier, T. Smy, J. Upham, R. W. Boyd, and S. Gupta, "Zero thickness sheet model of dispersive & nonlinear metasurfaces," in *2021 IEEE International Symposium on Antennas and Propagation and USNC-URSI Radio Science Meeting (APS/URSI)*, 2021, pp. 197–198.

[4] O. Reshef *et al.*, "Nonlinear plasmonic metasurfaces using multiresonant surface lattice resonances," in *2020 Conference on Lasers and Electro-Optics (CLEO)*, 2020, pp. 1–2.

[5] M. Z. Alam, S. A. Schulz, J. Upham, I. D. Leon, and R. W. Boyd, "Large optical nonlinearity of nanoantennas coupled to an epsilon-near-zero material," *Nature Photonics 2017 12:2*, vol. 12, pp. 79–83, 1 2018.

[6] S. Andreas, "Transparent conducting oxides—an up-to-date overview," *Mater*, vol. 5, pp. 661–683, 2012.

[7] J. Wu, Z. T. Xie, Y. Sha, H. Y. Fu, and Q. Li, "Epsilon-near-zero photonics: infinite potentials," *Photon. Res.*, vol. 9, no. 8, pp. 1616–1644, Aug 2021.

[8] Z. Hayran, J. B. Khurgin, and F. Monticone, "$\hbar\omega$ versus $\hbar k$: Dispersion and energy constraints on time-varying photonic materials and time crystals [Invited]," *Opt. Mater. Express*, vol. 12, no. 10, pp. 3904–3917, Oct 2022.

[9] Y. Zhou *et al.*, "Broadband frequency translation through time refraction in an epsilon-near-zero material," *Nature communications*, vol. 11, no. 1, pp. 1–7, 2020.

[10] H. Wang *et al.*, "Extended Drude model for intraband-transition-induced optical nonlinearity," *Physical Review Applied*, vol. 11, p. 1, 2019.

[11] R. W. Boyd, O. Reshef, E. Giese, M. Z. Alam, J. Upham, and I. D. Leon, "Beyond the perturbative description of the nonlinear optical response of highly nonlinear, epsilon-near-zero materials," *Optics InfoBase Conference Papers*, vol. Part F54-N, pp. 3–6, 2017.

[12] J. R. Zurita-Sánchez, P. Halevi, and J. C. Cervantes-González, "Reflection and transmission of a wave incident on a slab with a time-periodic dielectric function (t)," *Physical Review A - Atomic, Molecular, and Optical Physics*, vol. 79, p. 053821, 5 2009.

[13] J. R. Zurita-Sánchez, J. H. Abundis-Patiño, and P. Halevi, "Pulse propagation through a slab with time-periodic dielectric function $\epsilon(t)$," *Optics Express*, vol. 20, p. 5586, 2 2012.

[14] L. Zeng *et al.*, "Photonic time crystals," *Scientific Reports 2017 7:1*, vol. 7, pp. 1–9, 12 2017.

[15] C. Varin, G. Bart, R. Emms, and T. Brabec, "Saturable Lorentz model for fully explicit three-dimensional modeling of nonlinear optics," *Optics Express*, vol. 23, p. 2686, 2015.

[16] M. Moradi, S.-M. Pourangha, V. Nayyeri, M. Soleimani, and O. M. Ramahi, "Unconditionally stable fdtd algorithm for 3-d electromagnetic simulation of nonlinear media," *Optics Express*, vol. 27, p. 15018, 2019.

[17] D. F. Gordon, M. H. Helle, and J. R. Peñano, "Fully explicit nonlinear optics model in a particle-in-cell framework," *Journal of Computational Physics*, vol. 250, pp. 388–402, 2013.

[18] A. C. Ltd, "Flexible material plugins," Mar 2019. [Online]. Available: https://www.lumerical.com/learn/whitepapers/flexible-material-plugins/

[19] E. J. Rothwell and M. J. Cloud, *Electromagnetics*. CRC press, 2018.

[20] A. Taflove and S. C. Hagness, *Computational electrodynamics: The finite-difference time-domain method*, 3rd ed. Artech House, 2005.

[21] A. Z. Elsherbeni and V. Demir, *The finite-difference time-domain method for electromagnetics with MATLAB® simulations*, 2nd ed. IET, 2015.